

# Unsupervised Monocular Road Segmentation for Autonomous Driving via Scene Geometry

Sara Hatami Rostami  
K.N. Toosi University of Technology  
Tehran, Iran  
s.hatamirostami@email.kntu.ac.ir

Behrooz Nasihatkon  
K.N. Toosi University of Technology  
Tehran, Iran  
nasihatkon@kntu.ac.ir

## Abstract

*This paper presents a fully unsupervised approach for binary road segmentation (road vs. non-road), eliminating the reliance on costly manually labeled datasets. The method leverages scene geometry and temporal cues to distinguish road from non-road regions. Weak labels are first generated from geometric priors, marking pixels above the horizon as non-road and a predefined quadrilateral in front of the vehicle as road. In a refinement stage, temporal consistency is enforced by tracking local feature points across frames and penalizing inconsistent label assignments using mutual information maximization. This enhances both precision and temporal stability. On the Cityscapes dataset, the model achieves an Intersection-over-Union (IoU) of 0.82, demonstrating high accuracy with a simple design. These findings demonstrate the potential of combining geometric constraints and temporal consistency for scalable unsupervised road segmentation in autonomous driving.*

## 1. Introduction

Road detection and segmentation are among the most vital tasks in autonomous driving. Semantic segmentation serves as a major tool for this purpose, achieving high performance when trained in a supervised manner by leveraging densely annotated datasets [17, 26]. However, supervised semantic segmentation approaches rely heavily on pixel-wise annotations, which are costly and time-consuming to obtain [4]. To address the challenges of expensive and labor-intensive labeling, semi-supervised, weakly supervised, and unsupervised approaches have been explored. This study evaluates the effectiveness of a fully unsupervised approach for semantic segmentation of road scenes. While unsupervised methods are typically complemented by other approaches in safe autonomous driving pipelines, our aim here is to assess how well a fully unsupervised approach can perform on its own.

We propose a simple yet effective framework for processing road images captured by a calibrated camera mounted on a moving vehicle. The method classifies image pixels into road and non-road categories. In the first stage, a preliminary training phase is carried out using scene geometry. Specifically, all pixels above the horizon line are assumed to belong to non-road regions. Additionally, a rectangular region in front of the moving vehicle—corresponding to a quadrilateral in image coordinates—is identified as road-only, since it is unlikely to contain obstacles such as pedestrians or vehicles when the vehicle is moving at sufficient speed. The network is initially trained using these constraints while ignoring other regions.

In the second stage, the model is refined through temporal consistency constraints. Corresponding feature points are extracted and matched for pairs of consecutive frames, ensuring that pixels representing the same physical location across frames receive consistent labels. This step mitigates temporal inconsistencies in segmentation and improves model robustness.

The framework is model-agnostic and can be integrated with any segmentation architecture. In this study, we employ a lightweight CNN to enable efficient computation while maintaining high segmentation accuracy. The overall framework of the proposed approach is illustrated in Fig. 1, which depicts both the initial training phase and the subsequent refinement using temporal consistency constraints. In summary, our contributions are as follows:

- We leverage camera calibration and scene geometry to automatically generate weak labels, providing an initial structured signal for road vs. non-road segmentation.
- We introduce a mutual information-based temporal consistency loss that enforces stable predictions across consecutive frames by tracking local feature points.
- Our method achieves an IoU of 0.84 on the Cityscapes validation set, narrowing the gap to fine-tuned models (0.91 IoU), while requiring no labeled data.
- The framework is computationally lightweight, model-agnostic, and easily extendable to large-scale and dy-

dynamic autonomous driving scenarios.

## 2. Related Work

### 2.1. Unsupervised Semantic Segmentation

A significant line of research applies self-supervised learning to vision transformers (ViT), with DINO [3] pioneering this approach, marking a major advancement in unsupervised semantic segmentation (USS). Building on this, several recent methods [7, 13, 15, 27, 29, 34, 36] adopt a self-supervised pretrained ViT, i.e. DINO as their backbone. A prominent example is STEGO [7], which utilizes knowledge distillation to learn the correspondences between features extracted from DINO and introduces a novel contrastive loss function. There are other works that formulate unsupervised segmentation as a contrastive learning problem [2, 6, 7, 27]. For instance, Van Gansbeke et al. [6] propose a method that pulls pixel embeddings within the same object together, and pushes those from different objects apart. Beyond contrastive learning, another significant direction [1, 18, 20, 30, 34] explores spectral clustering for USS. For instance, FODVid [30] is an approach for unsupervised video object segmentation that uses DINO output features and the related optical flow to construct an adjacency graph, from which preliminary object masks are obtained via graph-cut.

### 2.2. Unsupervised Video Segmentation

Despite image segmentation models being usable for videos by processing them frame-by-frame, doing this ignores valuable temporal information available in frame sequences. Research on unsupervised video segmentation has mainly focused on unsupervised video object segmentation (VOS). AGS [33] links the near frames using a dynamic attention mechanism. The RTNet [23] approach involves reciprocally transforming appearance features to motion features, to mitigate the impact of misleading motion information on identifying primary objects. HFAN [22] is a hierarchical feature alignment network that aligns appearance and motion features with primary object semantics. PMN [14] generates component prototypes from RGB images and optical flow maps to capture both appearance and motion cues. MTNet [37] incorporates a temporal transformer module to model long-range temporal dependencies and improve frame-to-frame interaction.

### 2.3. Mutual Information For Unsupervised Semantic Segmentation

Mutual information maximization is a powerful principle in discovering structure in visual data without manual annotations. One notable method also employed in this paper is Invariant Information Clustering (IIC) [11]. IIC maximizes mutual information between paired image repre-

sentations—an image and its transformed version—to improve clustering performance while mitigating mode collapse. Another approach [35] incorporates a mutual information loss within a joint framework that estimates scene depth, camera motion, and road segmentation. The work by Ouali et al. [21] maximizes the mutual information between pairs of predictions obtained from two valid input orderings using different masked convolutions. InfoSeg [8] segments images by maximizing the mutual information between local and global high-level features obtained from a self-supervised model. These approaches demonstrate the versatility of mutual information as a training signal, and our work builds on this line of research.

### 2.4. Road Segmentation with Minimum Supervision

Recent research in road segmentation has increasingly focused on reducing or even eliminating the need for dense manual annotations. Several works have explored unsupervised segmentation in urban scenes. Unsupervised methods exploit geometry cues such as depth [29, 35] and cross-modal distillation [32]. Weakly-supervised approaches instead use limited signals such as pseudo-labels or image-level tags [10, 12, 24]. Tsutsui et al. [31] minimize supervision by exploiting weak signals such as a location prior and homogeneous texture cues to generate pseudo-labels for free-space segmentation. Robinet et al. [25] rely on this method and train a neural network to generalize past the label noise using Co-Teaching. These efforts show how road segmentation can be learned with surprisingly little supervision, paving the way for approaches that balance annotation efficiency with competitive accuracy.

## 3. Proposed Approach

### 3.1. Geometry-Driven Partial Masks

In the initial stage of training, we specify a region on the image that almost surely belongs to the road region. To do this, we consider a rectangular region on the ground in the road scene whose width is equal to the width of the car and extends from 2 to 5 meters in front of the car. In Cityscapes the origin of the vehicle coordinate system is assumed to be located on the ground directly beneath the center of the rear axle, with the X-axis pointing forward, the Y-axis pointing to the left, and the Z-axis pointing upwards [5]. Therefore, the four 3D corner points of this rectangle are  $[A+2, \pm w/2, 0]$  and  $[A+5, \pm w/2, 0]$  in vehicle coordinates, where  $w$  is the car width, and  $A$  is the distance between the rear axle and the front bumper of the car. These points are projected onto the image using the camera projection matrix, yielding a quadrilateral region in image coordinates, as shown in Fig. 2. This region reliably corresponds to the road, provided that the vehicle is moving fast enough

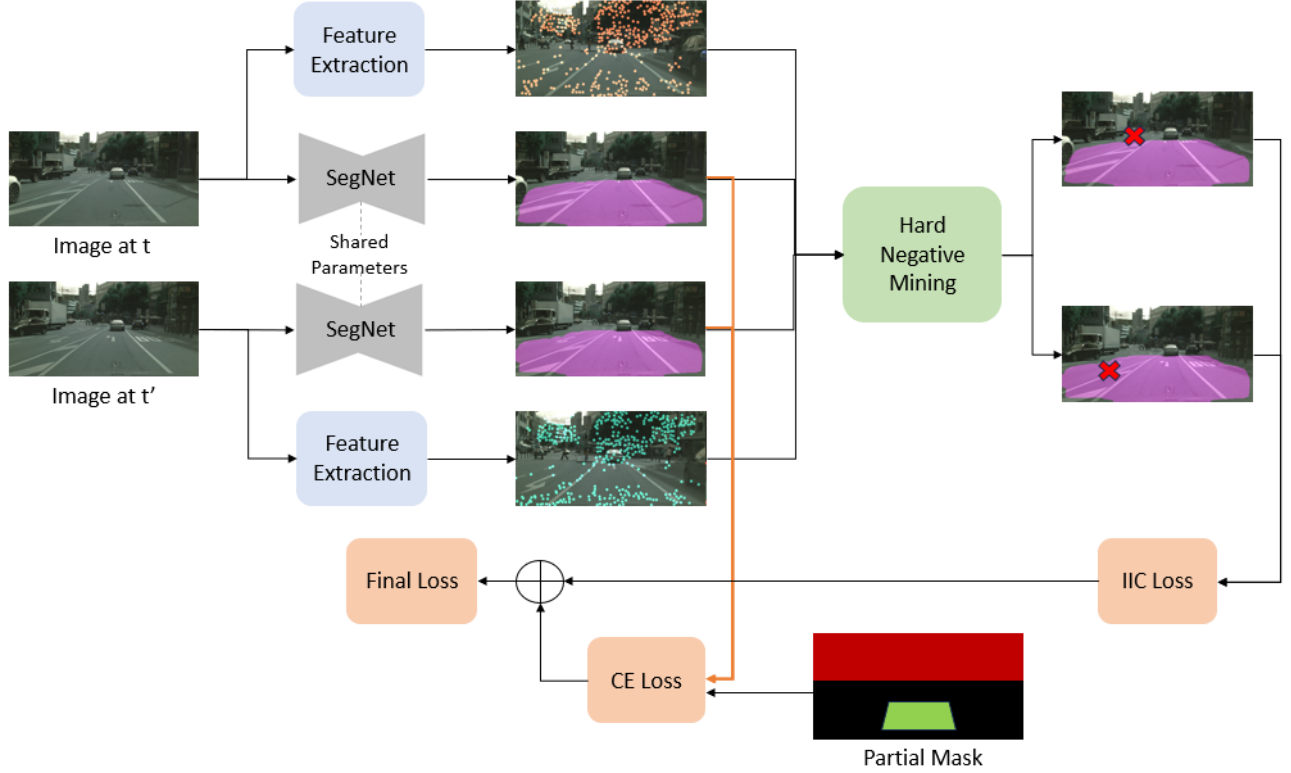


Figure 1. Overall framework of the proposed approach: initial training with partial mask and subsequent refinement with feature extraction and temporal consistency constraints. Feature extraction consists of corner detection and tracking across frames. The tracked corners are then filtered through hard negative mining before being fed into the IIC loss [11]. Finally, the IIC loss is combined with the cross-entropy loss to form the final loss for training the segmentation network.

so that transient obstacles (e.g., pedestrians or other vehicles) are unlikely to remain in this short-range area across consecutive frames. Consequently, all pixels lying inside this quadrilateral are labeled as road. In addition, we estimate the horizon line by considering a line at infinity lying on the ground plane in vehicle coordinates and projecting it through the camera projection matrix, thereby obtaining the image coordinates of the horizon line. Every pixel above this line is then labeled as non-road. Pixels outside these two designated regions are excluded from labeling to avoid introducing unreliable information. The external calibration parameters between the camera and vehicle coordinates are provided by the Cityscapes dataset. Given intrinsic and extrinsic parameters, the horizon line and the road region in image coordinates can be computed using the projection matrix  $Projection = K[R, t]$ , derived from the camera's calibration matrix  $K$  and the rotation matrix  $R$  and translation vector  $t$  between the vehicle and camera coordinates:

$$R = R_{V \rightarrow C} = R_{C \rightarrow V}^T = (R_z(\psi)R_y(\theta)R_x(\phi))^T \quad (1)$$

and

$$t = -Rt_{C \rightarrow V} \quad (2)$$

where  $R_{V \rightarrow C}$  is the rotation from the vehicle frame to the camera frame, and  $R_x(\phi)$ ,  $R_y(\theta)$  and  $R_z(\psi)$  are rotation matrices about the x-, y-, and z-axes, corresponding to roll, pitch, and yaw angles.  $t_{C \rightarrow V}$  denotes the translation vector from the camera frame to the vehicle frame.

### 3.2. Initial Training with Geometric Constraints

The initial training phase enforces the geometric constraints by optimizing a binary cross-entropy (BCE) loss function defined only on the rectangular road region and the region above the horizon:

$$\begin{aligned} \mathcal{L}_{\text{geometric}} = & -\frac{1}{N} \sum_{i \in R} \log \sigma(y_i) \\ & -\frac{1}{M} \sum_{i \in H} \log (1 - \sigma(y_i)) \end{aligned} \quad (3)$$

where  $y_i$  is the output of the network for pixel  $i$ , and  $\sigma$  is the sigmoid function, and consequently,  $\sigma(y_i)$  is the predicted probability of being road. The loss function is computed for the road region ( $R$ ) and the non-road region above the horizon ( $H$ ) in the partial mask.  $N$  and  $M$  are the number of

pixels in the road and non-road regions, respectively. The network learns to predict higher probabilities for drivable surfaces and lower probabilities for areas that are unlikely to be road. This initial training helps the model start with a reasonable understanding of the scene, making later training stage more effective.

### 3.3. Temporal Consistency and Feature Tracking

After the initial training phase, the model is refined by enforcing temporal consistency across video frames. First, feature points are extracted using the Shi-Tomasi corner detection algorithm [28]. Then these points are tracked across consecutive frames using the Lucas-Kanade optical flow method [19]. We then refine the training process by forcing the network to assign identical labels to a feature point and its tracked correspondence across frames, using mutual information maximization via the IIC loss [11]. Consider a set of feature point locations  $\mathbf{x}_1, \mathbf{x}_2, \dots, \mathbf{x}_n$  in image  $I$  and their tracked counterparts  $\mathbf{x}'_1, \mathbf{x}'_2, \dots, \mathbf{x}'_n$  in image  $I'$ .

Let  $y_i$  and  $y'_i$  denote the network output logits on  $I$  and  $I'$  at pixel locations  $\mathbf{x}_i$  and  $\mathbf{x}'_i$ , respectively. Let  $\mathbf{s}_i = [1 - \sigma(y_i), \sigma(y_i)]^T$  and  $\mathbf{s}'_i = [1 - \sigma(y'_i), \sigma(y'_i)]^T$  be the vectors of class probabilities, where  $\sigma(\cdot)$  represents the sigmoid function. To compute the IIC loss we first obtain the joint distribution matrix

$$\mathbf{P} = \frac{1}{n} \sum_{i=1}^n \mathbf{s}_i (\mathbf{s}'_i)^T \in \mathbb{R}^{2 \times 2}. \quad (4)$$

Then we compute the marginal distributions  $\mathbf{p}, \mathbf{p}' \in \mathbb{R}^2$  by summing over the rows and columns of  $\mathbf{P}$  respectively. Now, the IIC loss [11] can be evaluated by substituting the joint probability matrix  $\mathbf{P}$  into the mutual information expression:

$$\mathcal{L}_{\text{Consistency}} = -I(\mathbf{P}) = - \sum_{i=1}^2 \sum_{j=1}^2 P_{ij} \cdot \ln \frac{P_{ij}}{\mathbf{p}_i \cdot \mathbf{p}'_j}. \quad (5)$$

The final loss function combines the initial geometric constraints with the temporal consistency loss:

$$\mathcal{L}_{\text{Final}} = \mathcal{L}_{\text{Geometric}} + \mathcal{L}_{\text{Consistency}} \quad (6)$$

This ensures that the network not only respects the initial geometric priors but also produces temporally coherent predictions across video sequences.

### 3.4. Hard Negative Mining

In the refinement stage, inspired by hard negative mining, we focus training on temporally inconsistent feature points to refine the model’s decision boundaries. After each epoch, pairs of tracked points whose predicted labels differ across consecutive frames are flagged as inconsistent (see Fig. 2). Each epoch involves two steps: (1) extracting new inconsistent correspondences based on the current model, and (2)

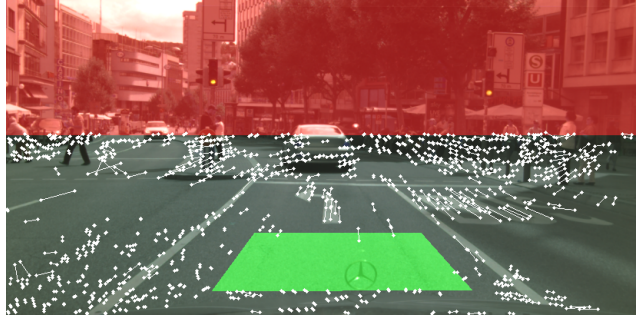


Figure 2. A frame from the Cityscapes dataset with its partial mask and point tracking results. The green area represents the road, while the red area denotes non-road regions. Selected pairs of tracked points with inconsistent labels predicted by the network after the 10th epoch are highlighted.

retraining with these updated pairs to improve segmentation accuracy. This iterative process continues until temporal inconsistencies are minimized, yielding a stable and robust segmentation model.

## 4. Experiments

### 4.1. Dataset

To evaluate the performance of our method, we utilized the Cityscapes dataset [5], which offers a comprehensive collection of urban driving scenes captured in Germany and is designed to benchmark segmentation methods for autonomous driving applications. For training, we employed 2,900 sequential frames from the Cityscapes dataset. For evaluation, depending on the procedure of the baseline methods, we use both the Cityscapes test set and the validation set, comprising 1,525 and 500 images, respectively.

### 4.2. Implementation Details

The segmentation model was implemented using a Lite R-ASPP network with a MobileNetV3-Large backbone [9], chosen for its lightweight design, computational efficiency, and strong performance in semantic segmentation tasks. The training process was carried out in two phases, utilizing an NVIDIA T4 GPU. In the first training phase, the network was trained for 100 epochs on sequential frames from the Cityscapes dataset, using the calculated horizon line and quadrilateral road region to enforce labels derived from these geometric constraints, which took approximately 210 minutes. In the second phase, the cost function was updated to include the temporal consistency loss, which enforced label consistency across corresponding pixels in adjacent frames. The updated network was trained 10 cycles, each consisting of 100 epochs and requiring approximately 300 minutes. To improve efficiency, only a subset of frame pairs was used during this stage of training. Instead of pro-

Method	IoU	Dataset
Joint Depth-Pose-Ground Learning [35]	0.83	Validation
Co-Teaching [25]	0.82	Validation
Transfer Learning	0.91	Validation
Proposed Unsupervised Method (Ours)	0.84	Validation
Video Segmentation [31]	0.78	Test
Weakly-Supervised [31]	0.85	Test
Proposed Unsupervised Method (Ours)	0.82	Test

Table 1. Performance comparison of the proposed unsupervised method with existing approaches on validation and test sets of Cityscapes.

cessing every consecutive frame, pairs were selected with a 5-frame interval, ensuring sufficient temporal variation, and frames with vehicle speeds below a certain threshold were excluded, so that obstacles such as pedestrians or other vehicles within the quadrilateral region would not affect the geometric labeling. In both training phases, the initial learning rate was set to  $1 \times 10^{-4}$ , and the Adam optimizer was used for stable convergence.

### 4.3. Evaluation of the Proposed Method

The performance of the proposed method was assessed using the Intersection-over-Union (IoU) metric, which is widely regarded as the most reliable measure of segmentation accuracy. We first compare our unsupervised approach with a supervised baseline. The same LR-ASPP model, initialized with COCO-pretrained weights [16], was trained on Cityscapes in an unsupervised manner. This baseline achieved an IoU of 0.91, while our fully unsupervised method reached 0.84 on the Cityscapes validation set (Tab. 1). The modest gap of 0.07 highlights the effectiveness of our fully unsupervised framework, especially considering that it requires no manual labeling.

For broader evaluation, we also compare our method with other existing approaches. Because our method is based solely on the loss function and remains agnostic to the segmentation network architecture, a fair comparison can only be made with methods that use the same architecture. However, we have included comparisons with approaches employing larger segmentation models. Since prior work report road segmentation performance on either the validation or test set, we include results on both for a fair comparison (Tab. 1). To further evaluate the effectiveness of the proposed method, we compare its performance with the weakly-supervised free-space segmentation method [31], which achieved strong results on road segmentation for the test set. As shown in Tab. 1, our unsupervised framework achieves slightly lower IoU than the weakly-supervised baseline. This is expected because our approach is fully unsupervised and simple, relying only on

Method	IoU
Trained with Geometric Constraints	0.74
Without Hard Negative Mining	0.80
With Hard Negative Mining	0.84

Table 2. Performance comparison between the initial training phase and the refinement stage, with and without hard negative mining, on the validation set.

geometric and temporal constraints. Despite its simplicity, it provides a strong and efficient baseline for road segmentation.

**Visual Analysis and Interpretation.** The qualitative results of the segmentation outputs further illustrate the effectiveness of the proposed method. Fig. 3 presents several examples of road segmentation outputs on images from Cityscapes. The model successfully delineates drivable areas with notably high precision, effectively distinguishing between road surfaces and non-drivable regions. The illustrated results highlights the model’s ability to adapt to varying road textures, lighting conditions, and perspectives. The robustness of the proposed method is attributed to its two-stage training approach. First, geometric constraints provide an initial structured learning signal, ensuring that the network understands fundamental road structures. Second, temporal consistency loss refines segmentation by leveraging frame-to-frame feature correspondence, leading to smoother and more coherent predictions over time. Minor inaccuracies are observed in challenging areas, such as vehicle tires and sidewalks, where the lack of explicit supervision may lead to occasional misclassifications, which could be further improved by integrating a small amount of annotations in future research. Nonetheless, the model consistently captures the general road structure with high fidelity. The results suggest that unsupervised learning with geometric and temporal cues is a promising direction for road segmentation in autonomous driving.

### 4.4. Ablation Study

Tab. 2 illustrates the impact of *temporal consistency* and *hard negative mining*. In the first training phase, the network was trained solely using geometric constraints as supervisory signals via partial masks, achieving an IoU of 0.74. Subsequent training with temporal consistency, but without hard negative mining, while utilizing all consistent and inconsistent feature points, increased the IoU to 0.80. Incorporating hard negative mining further improved accuracy to 0.84 while reducing the training time by half. These results indicate that hard negative mining enhances both efficiency and performance by directing the learning process toward the most informative and challenging mistakes.

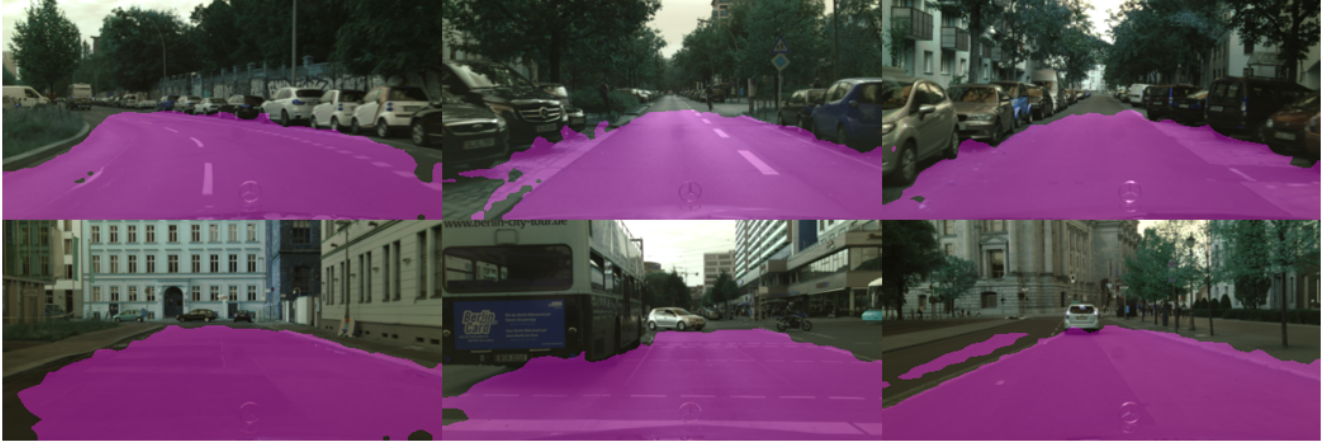


Figure 3. Examples of segmented Cityscapes images using the presented method

## 5. Conclusion

This study introduced a novel, fully unsupervised framework for road segmentation using a single monocular camera. The method leverages scene geometry and temporal consistency constraints to train a segmentation network without requiring any labeled data. Our method operates purely on the loss function and is therefore agnostic to the underlying segmentation architecture. Trained sequentially with geometric and temporal consistency objectives, the model produces stable and accurate segmentation on unseen Cityscapes test data. This performance demonstrates that strong results can be obtained with a lightweight CNN while entirely eliminating manual annotation. Compared to existing unsupervised approaches, the proposed framework is computationally efficient, relying on simple geometric priors and point tracking rather than costly pseudo-labeling, and exhibits strong generalization beyond dataset-specific conditions. Future work could further enhance performance by integrating weak supervision or domain adaptation strategies to improve robustness across diverse road environments.

## References

- [1] Amit Aflalo, Shai Bagon, Tamar Kashti, and Yonina Eldar. Deepcut: Unsupervised segmentation using graph neural networks clustering. In *ICCV*, pages 32–41, 2023. 2
- [2] Dong Bao, Jun Zhou, Gervase Tuxworth, Jue Zhang, and Yongsheng Gao. Hierarchical context learning of object components for unsupervised semantic segmentation. *Pattern Recognition*, 167:111713, 2025. 2
- [3] Mathilde Caron, Hugo Touvron, Ishan Misra, Hervé Jégou, Julien Mairal, Piotr Bojanowski, and Armand Joulin. Emerging properties in self-supervised vision transformers. In *ICCV*, pages 9650–9660, 2021. 2
- [4] Liang-Chieh Chen, George Papandreou, Iasonas Kokkinos, Kevin Murphy, and Alan L. Yuille. Deeplab: Semantic image segmentation with deep convolutional nets, atrous convolution, and fully connected crfs. *IEEE TPAMI*, 40(4):834–848, 2017. 1
- [5] Marius Cordts, Mohamed Omran, Sebastian Ramos, Timo Rehfeld, Markus Enzweiler, Rodrigo Benenson, Uwe Franke, Stefan Roth, and Bernt Schiele. The cityscapes dataset for semantic urban scene understanding. In *CVPR*, pages 3213–3223, 2016. 2, 4
- [6] Wouter Van Gansbeke, Simon Vandenhende, Stamatios Georgoulis, and Luc Van Gool. Unsupervised semantic segmentation by contrasting object mask proposals. In *ICCV*, pages 10052–10062, 2021. 2
- [7] Mark Hamilton, Zhoutong Zhang, Bharath Hariharan, Noah Snavely, and William T. Freeman. Unsupervised semantic segmentation by distilling feature correspondences. *arXiv preprint arXiv:2203.08414*, 2022. 2
- [8] Robert Harb and Patrick Knöbelreiter. Infoseg: Unsupervised semantic image segmentation with mutual information maximization. In *DAGM German Conference on Pattern Recognition*, pages 18–32, 2021. 2
- [9] Andrew Howard, Mark Sandler, Grace Chu, Liang-Chieh Chen, Bo Chen, Mingxing Tan, Weijun Wang, Yukun Zhu, Ruoming Pang, Vijay Vasudevan, Quoc V. Le, and Hartwig Adam. Searching for mobilenetv3. In *ICCV*, pages 1314–1324, 2019. 4
- [10] Dongbo Huang, Hui Wang, Yuqian Zhao, Feifei Guo, Fan Zhang, Pei Chen, Chunhua Yang, and Weihua Gui. Weakly supervised free-space segmentation by fusing spatial priors and region features for auto-driving. *Multimedia Systems*, 31(4):273. 2
- [11] Xu Ji, Joao F. Henriques, and Andrea Vedaldi. Invariant information clustering for unsupervised image classification and segmentation. In *ICCV*, pages 9865–9874, 2019. 2, 3, 4
- [12] Dongseob Kim, Seungho Lee, Junsuk Choe, and Hyunjung Shim. Weakly supervised semantic segmentation for driving scenes. In *Proceedings of the AAAI Conference on Artificial Intelligence*, pages 2741–2749, 2024. 2
- [13] Jiyoung Kim, Kyuhong Shim, Insu Lee, and Byonghyo Shim. Expand-and-quantize: unsupervised semantic seg-

- mentation using high-dimensional space and product quantization. In *AAAI*, pages 2768–2776, 2024. 2
- [14] Minhyeok Lee, Suhwan Cho, Seunghoon Lee, Chaewon Park, and Sangyoun Lee. Unsupervised video object segmentation via prototype memory network. In *WACV*, pages 5924–5934, 2023. 2
- [15] Kehan Li, Zhennan Wang, Zesen Cheng, Runyi Yu, Yian Zhao, Guoli Song, Chang Liu, Li Yuan, and Jie Chen. Acseg: Adaptive conceptualization for unsupervised semantic segmentation. In *CVPR*, pages 7162–7172, 2023. 2
- [16] Tsung-Yi Lin, Michael Maire, Serge Belongie, James Hays, Pietro Perona, Deva Ramanan, Piotr Dollár, and C. Lawrence Zitnick. Microsoft coco: Common objects in context. In *ECCV*, pages 740–755, 2014. 5
- [17] Jonathan Long, Evan Shelhamer, and Trevor Darrell. Fully convolutional networks for semantic segmentation. In *CVPR*, pages 3431–3440, 2015. 1
- [18] Qinghong Lin; Weichan Zhong; Jianglin Lu. Deep superpixel cut for unsupervised image segmentation. In *ICPR*, pages 8870–8876, 2020. 2
- [19] Bruce D Lucas and Takeo Kanade. An iterative image registration technique with an application to stereo vision. In *IJCAI’81: 7th international joint conference on Artificial intelligence*, pages 674–679, 1981. 4
- [20] Luke Melas-Kyriazi, Christian Rupprecht, Iro Laina, and Andrea Vedaldi. Deep spectral methods: A surprisingly strong baseline for unsupervised semantic segmentation and localization. In *CVPR*, pages 8364–8375, 2022. 2
- [21] Yassine Ouali, Céline Hudelot, and Myriam Tami. Autoregressive unsupervised image segmentation. In *ECCV*, pages 142–158, 2020. 2
- [22] Gensheng Pei, Fumin Shen, Yazhou Yao, Guo-Sen Xie, Zhenmin Tang, and Jinhui Tang. Hierarchical feature alignment network for unsupervised video object segmentation. In *ECCV*, pages 596–613, 2022. 2
- [23] Sucheng Ren, Wenxi Liu, Yongtuo Liu, Haoxin Chen, Guoqiang Han, and Shengfeng He. Reciprocal transformations for unsupervised video object segmentation. In *CVPR*, pages 15455–15464, 2021. 2
- [24] François Robinet and Raphaël Frank. Refining weakly-supervised free space estimation through data augmentation and recursive training. In *Artificial Intelligence and Machine Learning*, pages 30–45, 2022. 2
- [25] François Robinet, Claudia Parera, Christian Hundt, and Raphaël Frank. Weakly-supervised free space estimation through stochastic co-teaching. In *WACV*, pages 618–627, 2022. 2, 5
- [26] Olaf Ronneberger, Philipp Fischer, and Thomas Brox. U-net: Convolutional networks for biomedical image segmentation. In *MICCAI*, pages 234–241, 2015. 1
- [27] Hyun Seok Seong, WonJun Moon, SuBeen Lee, and Jae-Pil Heo. Leveraging hidden positives for unsupervised semantic segmentation. In *CVPR*, pages 19540–19549, 2023. 2
- [28] Jianbo Shi and Carlo Tomasi. Good features to track. In *1994 Proceedings of IEEE conference on computer vision and pattern recognition*, pages 593–600, 1994. 4
- [29] Leon Sick, Dominik Engel, Pedro Hermosilla, and Timo Ropinski. Unsupervised semantic segmentation through depth-guided feature correlation and sampling. In *CVPR*, pages 3637–3646, 2024. 2
- [30] Silky Singh, Shripad Deshmukh, Mausoom Sarkar, Rishabh Jain, Mayur Hemani, and Balaji Krishnamurthy. Fodvid: flow-guided object discovery in videos. *arXiv preprint arXiv:2307.04392*, 2023. 2
- [31] Satoshi Tsutsui, Tommi Kerola, Shunta Saito, and David J. Crandall. Minimizing supervision for free-space segmentation. In *CVPR*, pages 988–997, 2018. 2, 5
- [32] Antonin Vobecky, David Hurych, Oriane Siméoni, Spyros Gidaris, Andrei Bursuc, Patrick Pérez, and Josef Sivic. Drive & segment: Unsupervised semantic segmentation of urban scenes via cross-modal distillation. In *ECCV*, pages 478–495, 2022. 2
- [33] Wenguan Wang, Hongmei Song, Shuyang Zhao, Jianbing Shen, Sanyuan Zhao, Steven C. H. Hoi, and Haibin Ling. Learning unsupervised video object segmentation through visual attention. In *CVPR*, pages 3064–3074, 2019. 2
- [34] Yangtao Wang, Xi Shen, Shell Xu Hu, Yuan Yuan, James L. Crowley, and Dominique Vaufreydaz. Self-supervised transformers for unsupervised object discovery using normalized cut. In *CVPR*, pages 14543–14553, 2022. 2
- [35] Lu Xiong, Yongkun Wen, Yuyao Huang, Junqiao Zhao, and Wei Tian. Joint unsupervised learning of depth, pose, ground normal vector and ground segmentation by a monocular camera sensor. *Sensors*, 20(13):3737, 2020. 2, 5
- [36] Zhaoyuan Yin, Pichao Wang, Fan Wang, Xianzhe Xu, Hanling Zhang, Hao Li, and Rong Jin. Transfgu: A top-down approach to fine-grained unsupervised semantic segmentation. In *ECCV*, pages 73–89, 2022. 2
- [37] Yunzhi Zhuge, Hongyu Gu, Lu Zhang, Jinqing Qi, and Huchuan Lu. Learning motion and temporal cues for unsupervised video object segmentation. *IEEE Transactions on Neural Networks and Learning Systems*, 36(5):9084–9097, 2024. 2